ACS APPLIED MATERIALS & INTERFACES

Research Article

www.acsami.org

Low-Cost Thermo-Optic Imaging Sensors: A Detection Principle Based on Tunable One-Dimensional Photonic Crystals

Armin T. Exner,[†,§] Ida Pavlichenko,[‡,§] Bettina V. Lotsch,[‡] Giuseppe Scarpa,[†] and Paolo Lugli*[,†]

[†]Institute for Nanoelectronics, Technische Universität München, Arcisstrasse 21, D-80333 Munich, Germany

[‡]Max Planck Institute for Solid State Research, Heisenbergstrasse 1, D-70569 Stuttgart, Germany, and Department of Chemistry, Ludwig-Maximilians-Universität (LMU), Butenandtstrasse 5-13 (D), D-81377 Munich, Germany

Supporting Information

ABSTRACT: Infrared (IR) sensors employing optical readout represent a promising class of devices for the development of thermographic imagers. We demonstrate an infrared radiation detection principle based on thermally tunable one-dimensional (1D) photonic crystals acting as optical filters, integrated with organic and inorganic light emitting diodes (OLEDs and LEDs, respectively). The optical filters are composed of periodically assembled mesoporous TiO_2 and SiO_2 layers. Due to the thermal tunability of the transmission spectrum of the optical filter, the intensity of light passing through the filter is modulated by temperature. The tuned spectrum lies in the visible region and, therefore, can be directly detected by a visible-light photodetector. The thermal response of the luminance of the OLED-photonic crystal ensemble is 3.8 cd m^{-2} K^{-1}. Furthermore, we demonstrate that the local temperature profile can be time and spatially resolved with a resolution of 530 by 530 pixel, thus enabling a potential application as an infrared imaging sensor featuring low power consumption and low fabrication costs.

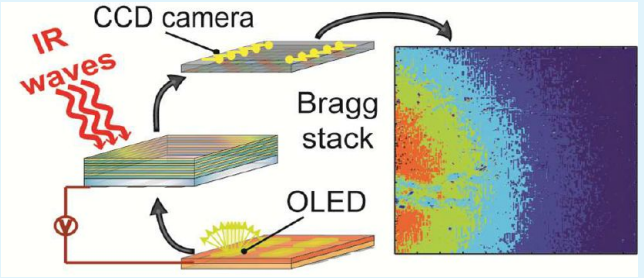

KEYWORDS: *infrared sensors, photonic crystals, Bragg stacks, OLED, LED, thermo-optic effect*

INTRODUCTION

Infrared imaging is one of the paramount tools for a contact-free temperature measurement of solid and fluid systems in industrial and environmental processes, allowing for a plethora of applications for diagnostics in material and biomedical sciences.[1,2] Hitherto, various approaches have been proposed to realize infrared sensors, among which two subcategories have won major recognition: (i) photoelectric detectors and (ii) thermal detectors.[3,4] Photoelectric detectors convert incident infrared (IR) radiation into electrical charge through the internal photoelectric effect. These detectors exhibit the best signal-to-noise ratio and a fast response; however, they require cryogenic cooling, which adds up on their size, weight, and cost.[3,5,6] Besides, the typical materials for photoelectric IR sensors include semiconductors such as PbS, PbSe, InAs, InSb, PbSnTe, InGaAs, and most prominently the ternary alloy HgCdTe, which is epitaxially grown in high vacuum with photolithographic masking and etching processing steps, which additionally makes its realization complex and expensive.[7] The second category—thermal detectors—absorb IR radiation, which in turn produces a change in a specific physical property of a material, as in, for example, resistive bolometers or pyroelectric detectors.[8] Thermal detector technology exploits semiconducting materials[9] or thermally sensitive resistors, which exhibit a temperature coefficient of resistance ($\Delta R/\Delta T$) of about 4% per degree celcius.[10] Typical representatives are transition metal oxides such as VO_2, V_2O_5,[10−12] Mn_3O_4, NiO, and CoO,[7−10] polycrystalline silicon−germanium alloy ($polySi_{0.7}Ge_{0.3}$),[13] or micromachined bimetallic cantilevers.[14] Thermal detectors do not require cryogenic cooling and, therefore, are facile to use and have lower overall system costs.[15,16] Nonetheless, thermoresistive detectors require complicated etching techniques and membrane transfer bonding techniques, which implies many processing steps.[17,18] The sensitivity of a thermal detector is limited by the response of the active material and the overall noise of the system. In general, one needs materials where at least one parameter displays strong temperature dependence, as, for example, the electric resistance in the case of microbolometers.[19] Then, measurements via integrated electronics can be performed.[20]

Another possible approach exploits the changes in optical parameters of the sensitive element, e.g. its refractive index (RI), and, as a consequence, in its transmission/reflection properties. Such changes are readable by an optical setup or even by the bare eye. This principle may trigger the emergence of various IR sensor designs utilizing photonic structures, which would perform infrared thermography based on the "wavelength conversion" of IR radiation into light intensity changes in the visible range. The development of a new thermo-optic imaging technology can significantly decrease the system cost

Received: September 12, 2012
Accepted: January 3, 2013
Published: January 3, 2013

   dx.doi.org/10.1021/am301964y | ACS Appl. Mater. Interfaces 2013, 5, 1575−1582

by eliminating a dedicated electronics readout and multistep fabrication routines.[19] The price of a state-of-the-art bolometric IR camera currently reaches ≈30,000 USD (T620, FLIR IR camera) for a system with 0.3 megapixel resolution and is, therefore, a limiting factor for the application range of IR thermography.

Notably, the concept of optical readout for IR sensors has been proposed by several groups.[18,20−23] The demonstrated approaches rely mostly on optical deflection exhibited by temperature-sensitive microelectromechanical systems (MEMS) that are read out by constructing an interference pattern, which increases the system's cost and complexity. Another promising, yet technically challenging microphotonic IR detection principle was shown by Watts et al., namely, by combining high-Q micrometer-scale resonators with extreme thermal isolation for low-noise thermal detection.[24] A further step in the improvement of the existing sensor designs toward a lower cost production and direct read out by the eye can be achieved by employing photonic crystals (PCs)—periodic dielectric nanostructures capable of manipulating light owing to strong coherent scattering interactions.[25,26] Particularly, PCs with a photonic stop band—a forbidden range of frequencies of the photons—in the visible region of the spectrum, are potentially able to "translate" IR radiation into visible color changes. This concept was recently demonstrated by Pris et al.[27] who presented a novel type of a miniature ultrasensitive, fast, and heat-sink-free IR thermo-optic sensor inspired by natural photonic structures present in the *Morpho* butterfly, in which IR absorption is enhanced by modifying the wing structures with single-walled carbon nanotubes. However, a bioinspired fabrication of artificial wing structures is far from trivial; hence, simpler approaches toward producing less complex thermally responsive structures are desirable,[28] such as one-dimensional PCs—multilayer interference-based optical filters with a periodic modulation of the RI in one dimension.[29] These so-called Bragg stacks (BSs) can be assembled from thermally responsive materials in which the RIs are temperature-dependent owing to the thermo-optic effect (TOE). Therefore, the optical properties of BSs comprising thermo-optic materials can be tuned upon varying the temperature.[30,31] Consequently, thermally responsive optical filters can be used to tune the intensity of a narrow-band visible light source, for example, when integrated with an organic light-emitting diode. For example, the coupling of an OLED with IR sensitive materials has been realized by Kim et al.[32] The authors investigate a hybrid "up-conversion" device based on IR sensitive PbSe nanocrystals incorporated into a green phosphorescent OLED.

In this paper, we report a route toward producing a thermo-optic imaging sensor with a ternary architecture based on the integration of sol−gel processed thermoresponsive one-dimensional photonic crystals with an OLED or LED, respectively, and a high-resolution camera. The proposed IR sensing principle is based on visualizing the changes of the intensity of light, propagating from the light source through the Bragg stack. Detecting visible light can be done in a straightforward and inexpensive fashion with low noise by using commercially available charge-coupled device (CCD) or complementary metal oxide semiconductor (CMOS) imagers. In this respect, our approach goes beyond the standard photonic crystal detection schemes based on the registration of the spectral shift of the photonic stop band.[33,34]

RESULTS AND DISCUSSION

As a proof of concept, we demonstrate the universality of the proposed approach by using a commercially available narrow-band blue LED as a light emitter. By detecting the light intensity transmitted through the 1D PC as a function of temperature, the thermal tunability of the PC directly translates into the intensity modulation observed at the detector. The scheme of the experimental setup is demonstrated in Figure 1a. As can be seen, the light from the LED is sent through the collimator−monochromator system and afterward through the BS and detected by the photodetector. The LED has a spectral full width at half-maximum (fwhm) of 28 nm (the spectrum of the LED light, divided by five, is plotted in Figure 1b, black dotted line). In order to match the emission spectrum of the LED, a BS thickness parameter optimization was performed to obtain a BS with 50 nm TiO_2 and 90 nm SiO_2 layers (Figure 1b, red star line). In order to provide a steep stop band, the number of bilayers was chosen to be eight (the cross section scanning electron microscopy (SEM) image of the investigated BS can be found in Figure 2i). The transmission of the BS at 25 °C and at a wavelength of 464 nm is approximately 15%. The colored lines in Figure 1b represent the spectra of the light transmitted from the LED through the BS recorded at temperatures in the range from 10 to 50 °C with a step size of 5 °C. We observed that due to the filter function of the BS in the wavelength range 450−500 nm the peak wavelength of the transmitted LED light (Figure 1, blue, green, yellow, and red curves) is shifted by ≈10 nm into the red compared to the original 464 nm peak of the LED spectrum (black dotted line). The reason for this shift can be found in the shape of the stop band of the BS (Figure 1b, red star line). However, by slightly changing the optical thicknesses of the BS layers and, hence, its transmissive properties, the light output of the LED can be increased. The LED-BS transmission spectra in Figure 1 show a gradual increase in light intensity transmitted through the BS with rising temperature. Figure 1c shows the intensities of the emission peaks at various temperatures, namely, the value of the peak intensity increases from ≈11% for 10 °C to ≈20% for 50 °C. The intensity increase is observed due to the blue-shifting of the photonic stop band of the BS upon heating, which can be explained by considering the thermo-optic coefficients (TOCs) of the chosen materials of the BS's layers. Namely, the negative TOC of the bulk TiO_2 (equal to -1.77×10^{-4} K^{-1} between 18 and 120 °C and to -3.04×10^{-4} K^{-1} between 220 and 325 °C at 800 nm), in contrast to the lower positive TOC of bulk SiO_2 (1×10^{-5} K^{-1}) dominates the thermal response of the BS layers.[36] Consequently, the optical thickness of the TiO_2/SiO_2 bilayer *decreases* upon increasing temperature, and *vice versa*. Additionally, as pointed out elsewhere,[30] the ambient humidity also plays an amplifying role in the tuning behavior by enhancing the sensitivity of the BS. A detailed description of the dependence of the RI on temperature for nanoparticle-based silica and titania films can be found elswhere.[30] Thus, the nonlinear trend of the dependence of the intensity of the LED (see Figure 1b) on the temperature for temperatures below 20 °C originates from the effect of water adsorption/desorption into/from the BS.[30] This experiment demonstrates the easy readout of changes in the position of the stop band of an arbitrary BS by using a LED and a detector.

As a next step, we demonstrate a miniature integrated sensing platform developed by depositing the OLED and the BS on opposite sides of the same glass plate as shown in Figure

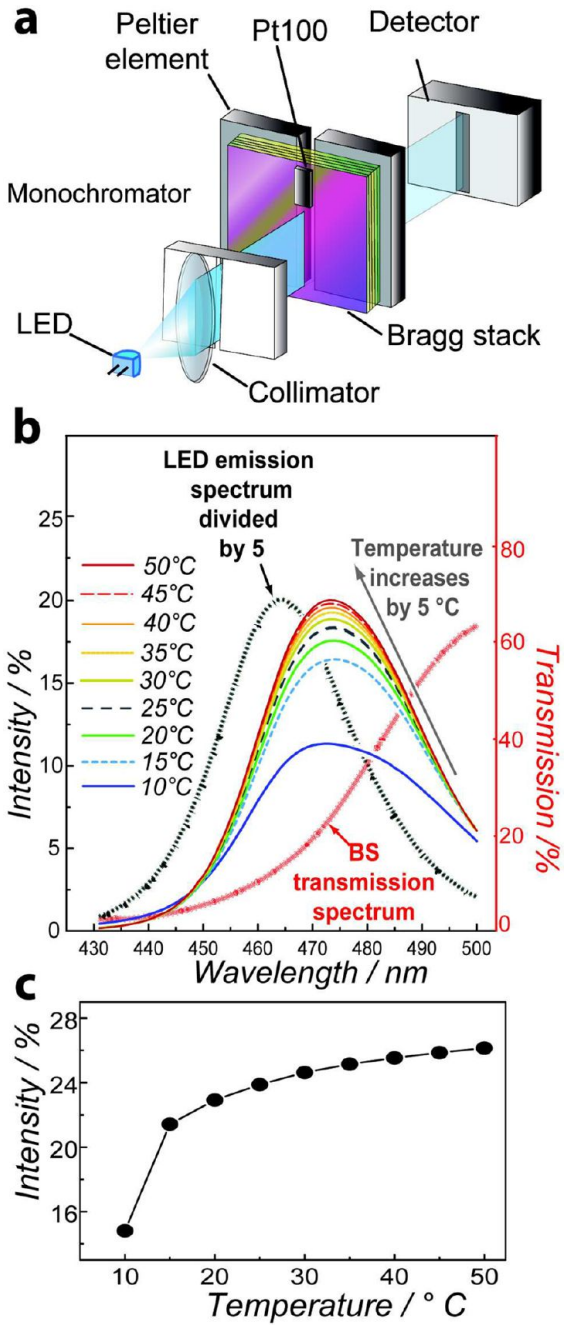

Figure 1. (a) Scheme of the experimental setup for the tuned LED light intensity. (b) Blue, green, yellow, and red lines demonstrate the intensity of light, transmitted from the blue LED through the BS with 8 TiO_2 (50 nm)/SiO_2 (90 nm) bilayers. The temperature is controlled between 10 and 50 °C in steps of 5 °C. As a reference, the LED spectrum (black dotted line) was scaled to the size of the graph ("Intensity" axis, left). The transmission spectrum of the BS (red star line) is plotted with respect to the "Transmission" axis (right). (c) Plot showing the dependence of the peak intensity derived from the LED-BS transmission spectra in part b on the temperature.

2a. The BS was fabricated via multiple sequential spin-coating of a high RI material—TiO_2 nanoparticles and a low RI material—commercially available SiO_2 nanoparticles (Figure 2i).[30,35] Alternatively, a titania sol and a mesoporous silica–surfactant sol was employed, allowing the preparation of high surface area mesoporous films via evaporation-induced self-assembly[37] (Figure 2ii). As mentioned earlier, TiO_2 and SiO_2 have been chosen for their high RI contrast on the one hand and the high TOC of TiO_2 on the other hand. The BSs, deposited onto the indium tin oxide (ITO) glass substrates, were integrated with polymer OLEDs assembled by spin-coating. An emissive OLED polymer PDY-132 was selected because of its good stability and match with the sensitivity range of the CCD camera. A more detailed description of the synthesis and fabrication steps can be found in the Supporting Information. As shown in Figure 3, the transmissive properties of the BS can be precisely tuned through optimizing the deposition parameters, such as spin-coating speed and acceleration, or the concentration of the suspensions, to match the emission spectrum of the OLED. The transmission through the BS can be measured by a photodiode, and the information about the light intensity distribution across the BS area can be obtained by, for example, a CCD or a CMOS active-pixel array camera (Figure 2b and c). The Bragg stack does not require a lithographic pixel fabrication as for most IR detectors, since the pixels are provided by the camera, recording the intensity distribution along the area of the coupled OLED-BS system.

Due to the thermal contact of the OLED with the BS, the temperature changes of the BS and the OLED are interrelated. Therefore, we independently investigated the influence of the temperature change on the emission properties of the OLED on the one hand and the BS's spectral shift on the other hand, as well as the thermal response of the coupled OLED-BS system.

To realize the intensity tuning of the light emitted by the OLED, we assembled a Bragg stack consisting of six bilayers of nanoparticle-based TiO_2 and SiO_2 layers (Figure 5c). The optimization of the thickness of the layers (60 nm for TiO_2 with RI ≈ 1.9 and 110 nm for SiO_2 with RI ≈ 1.3) allowed us to obtain a filter with a first-order photonic stop band between 490 and 640 nm, matching the emission spectrum of the polymer OLED lying in the range between 500 and 620 nm (Figure 3a and b). In Figure 3b, we demonstrate the shifting behavior of the photonic stop band of the BS upon heating in ambient conditions. Heating induces a change in the effective RI of the employed materials due to the combination of two phenomena operating simultaneously: The inherent thermo-optic effect and the desorption of the water molecules from the porous network of the BS lead to the change of the optical thickness of the layers and, thus, to a blue shift of the stop-band position.[30] The measurements were performed as described in the Supporting Information. The reversibility of the BSs thermal tuning is proven by the fact that measurements of the transmission curves at room temperature carried out before the heating and after the cooling cycles are the same. We observe a consistent blue shift of the stop band position upon increasing temperature, equal to 25 nm for the 40% transmission level in the temperature range from 15 to 35 °C, and if we follow the transmission values at a given wavelength in Figure 3b (the vertical gray dashed line at 560 nm), we observe a variation of the optical transmission of the filter from ≈10% to ≈28% upon heating. The shift for temperatures below ≈20 °C exhibits a nonlinear behavior due to the adsorption of ambient water into the BS's textural mesopores, which is more pronounced at lower temperatures closer to the dew point. As suggested in our previous study with similar BSs, the humidity of the ambient air plays a key role in enhancing the sensor response, giving rise to an "*effective*" TOE.[30] Using BSs composed of dense layers reduces or even completely eliminates the nonlinear shifting

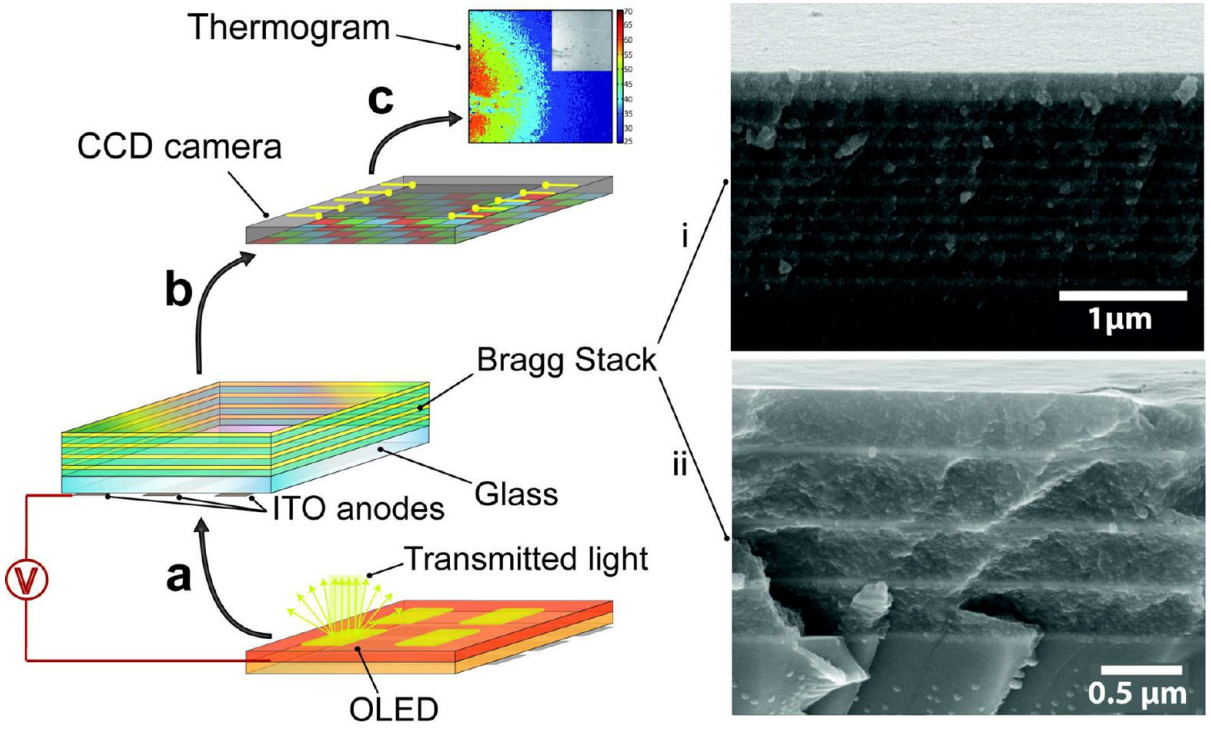

Figure 2. Scheme of the proposed thermo-optic imaging sensor featuring: (a) an OLED on the ITO-coated side of the glass substrate, (b) integration of the OLED-BS system with a CCD camera, and (c) visualization of the heat distribution on the surface of the OLED-BS ensemble. The BSs were made of (i) TiO_2 and SiO_2 nanoparticle-based layers and (ii) dense TiO_2 and mesoporous SiO_2 layers.

behavior caused by the presence of ambient humidity.[38] Note, however, that reducing the humidity contribution also leads to a drop in sensitivity of the device, rendering the use of materials with a sufficiently high TOC necessary.

In the next step, we investigate the temperature dependence of the optical emission properties of the OLED alone. As mentioned above, in the proposed setup geometry, the simultaneous heating of the OLED during the temperature increase of the BS cannot be avoided; therefore, the individual contributions of OLED and BS need to be analyzed separately. First, the OLED structure was fabricated on a glass plate and encapsulated as described in the Supporting Information. The active area of the OLED is equal to 3 mm × 3 mm with a light output of approximately 120 cd m^{-2}. A picture of the experimental setup is provided in Figure 4, showing a mounted OLED-BS system with a PT100 temperature sensor next to the active area. Figure 5a shows the emission spectrum of the OLED without BS for temperatures between 15 and 35 °C. In this temperature range we observe two phenomena related to the behavior of the emission spectra: (i) the intensity increases linearly upon rising temperature, and (ii) the peak intensity shifts about 1.5 nm into the blue, upon rising temperature. Both effects are fully reversible. The peak position has been determined by linear interpolation of the first derivative of the spectrum.

In the next step, a couple consisting of a BS and an OLED structure solution-processed on the opposite sides of a glass plate was assembled (see Figures 2 and 4). As indicated by the scheme in Figure 2a, the first step in the fabrication of the combined OLED-BS system is the fabrication of the Bragg stack on a glass substrate with the subsequent deposition of the OLED on the other, ITO-coated, surface of the glass substrate with the BS. Figure 5b shows the emission spectra of the OLED-BS at temperatures between 15 and 35 °C with a step size of 5 °C. We observe an enhanced tuning of the intensity compared to the native OLED. The temperature response unveils two trends in the behavior of the device: (i) the increase of the peak intensity by a factor of 1.6 in a temperature range from 15 to 35 °C (notably, this effect exceeds the performance of the single OLED, which increases only by a factor of 1.3), and (ii) the shift of the emission peak toward shorter wavelengths by 3 nm upon increasing temperature. The last observation can be explained by the effect of the BS shifting behavior, namely, 25 nm per 20 °C increase, which exceeds the shift of the OLED alone being only 1.5 nm.

In order to simplify the readout apparatus, we show that the temperature changes can be detected by the integrated light going through the BS with a setup as sketched in Figure 4b. The temperature was varied using a Peltier element, between 15 and 40 °C with a step size of 5 °C. This procedure was repeated three times to check its reproducibility. Figure 5c shows the temperature-induced modulation of the luminance (L) of the OLED alone and of the OLED-BS integrated device. The luminance of the OLED-BS device changed from 100.3 to 194.1 cd m^{-2} in a range from 15 to 40 °C. It is notable that L of the combined OLED-BS system increased linearly with temperature, with a rate dL/dT derived from the linear fit of the dependence of L on temperature, equal to 3.8 ± 0.1 cd m^{-2} K^{-1} over the whole temperature range. In contrast, the single OLED, tuned in the same temperature range, showed higher luminance values from 180.8 to 218.0 cd m^{-2}; however with 2.5 times lower sensitivity of 1.5 ± 0.1 cd m^{-2} K^{-1} in comparison with the coupled OLED-BS system. Thus, it can be seen that the thermal response of the integrated OLED-BS system is higher than that of the OLED alone. The displayed resolution of the luminance meter was 0.1 cd m^{-2}, this value exceeds the noise of the system and therefore is the limiting factor in the system precision. The resolvable temperature was calculated to

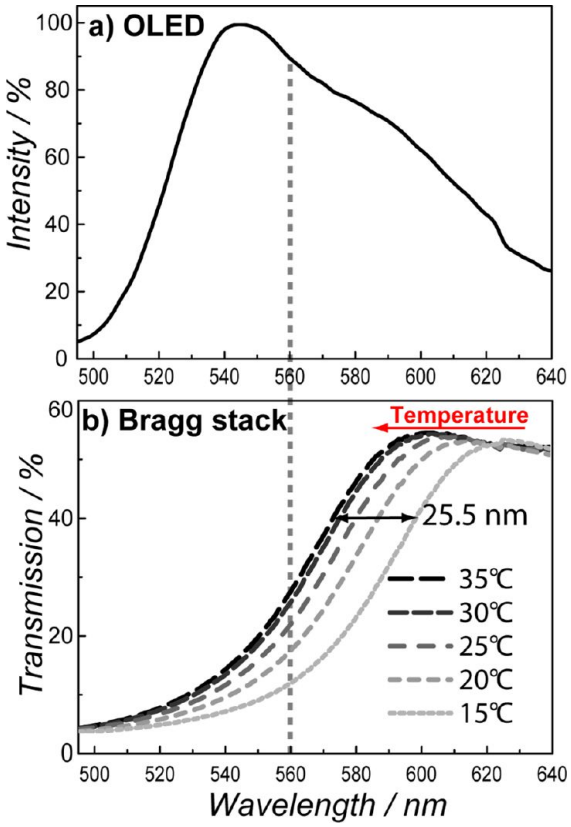

Figure 3. (a) Emission spectrum of the OLED. (b) Transmission spectra obtained upon heating a six bilayer TiO_2 (60 nm)/ SiO_2 (110 nm) BS from 15 to 35 °C with a step size of 5 °C. Note that the spectra of the BS match the OLED emission curve: the gray dashed line shows the change in the transmission from ≈10% to ≈28% at 560 nm corresponding to 90% emission of the OLED.

be 67 ± 3 mK for the OLED alone and 27 ± 3 mK for the OLED-BS system. The specifications are summarized in Table 1.

In order to demonstrate the feasibility of IR imaging we integrated the OLED-BS sensor with a camera detector array, as indicated in the scheme in Figure 2. We set up a commercial CCD camera above the device so that the light output can be recorded over the whole OLED-BS area with a resolution of 530 by 530 pixels. To detect the filter transmission in two dimensions, the light emission had to be homogeneous over the whole active filter area, a criterion verified by our OLED. The intensity of the transmitted light corresponds to the temperature of the respective point on the OLED-BS. In Figure 6a, we present a colored optical image of the OLED-BS equilibrated at 27 °C. The light intensity is relatively constant over the whole 3 × 3 mm large surface. The actual gray scale image as acquired from the CCD camera is shown in the upper right corner. Figure 6b shows a colored optical image of the OLED-BS under a temperature gradient induced by a hot source (here, a soldering iron at a temperature of 400 °C on the left side) generating a local temperature of less than 60 °C on the edge of the device. The increased light output shown by the monochrome image in the inset can also be seen by the naked eye. Figure 6c is taken 10 s after heating, when the device was at a temperature of 33 °C. All pictures show some irregularities in a micrometer range that originate from defects in the OLED top electrode morphology. Also slight irregularities on the surface are due to the fabrication imperfections and inhomogeneity of a BS. The inhomogeneities can be compensated by calibration and background correction, typical for IR-detectors.[39] In order to improve the readability of the image and to reduce the inhomogeneities, we subtracted the background intensity and calibrated the picture (a detailed description of the calibration procedure is given in the Supporting Information). The corrected image in Figure 7 outlines the gradual decrease of temperature with increased distance from the heat source position (the left edge). Figure 7 also indicates that a minimization of the thermal crosstalk has to be considered along with the device engineering. In principle, the crosstalk can be minimized by using thinner substrates or by separating the pixels by means of standard lithographic techniques. With this experiment, we prove that with the proposed thermo-optic intensity-tuning technique one can visualize the temperature changes of the integrated optical systems with a visible-light detector, such as a CCD array. Moreover, one can time and spatially resolve the kinetics of thermal equilibration and spreading of temperature fronts in the OLED-BS coupled devices. If a high temperature gradient is present, the sensor can be even be read out with the naked eye. The advantage of the introduced sensing scheme is that it involves low cost and noncomplicated fabrication methods and low power consumption (because the whole setup requires only an OLED powered at 4.5 V as the light source) and thus

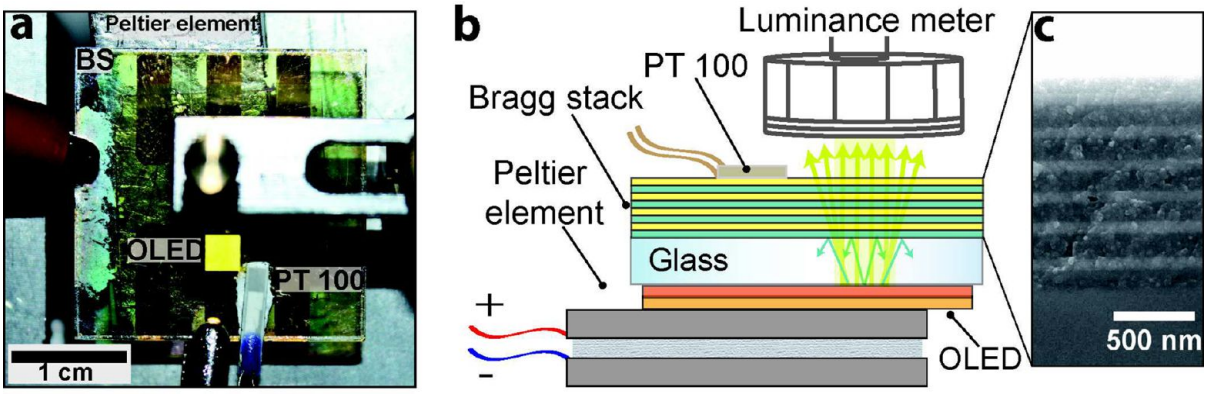

Figure 4. (a) Photograph of the sample holder with an emitting OLED-BS couple mounted onto the Peltier element. (b) Scheme of the experimental setup for the luminance measurements. (c) Cross-section SEM picture of the BS, composed of six bilayer SiO_2 (dark layers)/TiO_2 (bright layers).

dx.doi.org/10.1021/am301964y | ACS Appl. Mater. Interfaces 2013, 5, 1575−1582

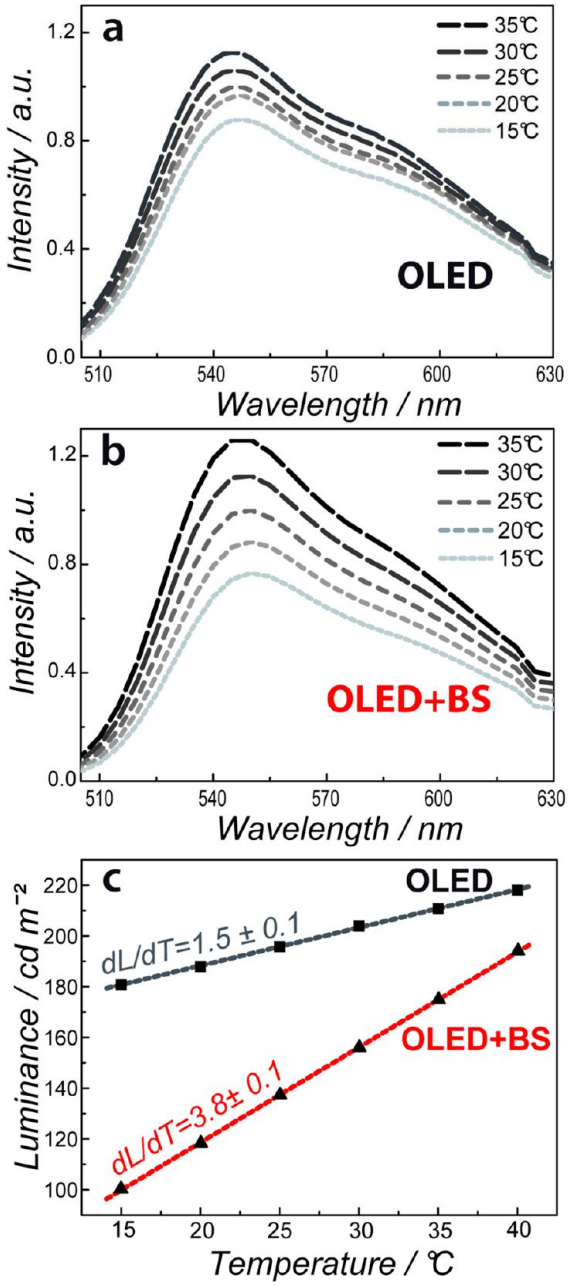

Figure 5. (a and b) The emission spectra of (a) the OLED alone and (b) the OLED-BS system recorded upon increasing the temperature from 15 to 35 °C in steps of 5 °C. For clarity, the intensities of the spectra are normalized with respect to the peak intensity at 25 °C. (c) Comparison of the luminance of the OLED alone and the OLED-BS system measured by a luminance meter. The single OLED exhibits a temperature coefficient dL/dT of 1.5 cd m^{-2} K^{-1}, whereas the combined OLED-BS device shows a 2.5 times higher sensitivity of dL/dT = 3.8 cd m^{-2} K^{-1}.

Table 1. Comparison of the Temperature Response and the Resolvable Temperature of the OLED and OLED-BS Systems

	sensitive area [mm]	power dissipation [mW]	temperature response [cd m^{-2} K^{-1}]	resolvable temperature [mK]
OLED	3 × 3	2	1.5 ± 0.1	67 ± 3
OLED-BS	3 × 3	2	3.8 ± 0.1	27 ± 3

represents a promising candidate for potential IR imaging detectors.

The hybrid OLED-BS device exhibits thermally tunable characteristics, thus enabling a versatile infrared imaging scheme. It should be mentioned that both OLED alone and the OLED-BS combination show pronounced thermal tunability and both are, therefore, possible candidates for IR image sensors. However, a coupled device consisting of an OLED and a Bragg stack is 2.5 times more sensitive toward temperature changes than the OLED alone. The achieved temperature sensitivity of 3.8 cd m^{-2} K^{-1}, equivalent to a temperature coefficient of luminance of 3.8%, can be compared with state-of-the-art thermoresistive detectors. For comparison, VO_2, which is often used in thermal detectors, has a temperature coefficient of resistance (TCR) of 4% for a single element cell.[1] We calculated the resolvable temperature to be 27 ± 3 mK for the measurement taken with the luminance meter. It is crucial to match the OLED and the BS such that the OLEDs emission peak wavelength is at the edge of the filter's stop band. The shift of the transmission depends on the effective TOE of the materials constituting the BS. The slope is determined by the refractive index contrast of the BS materials and the number of bilayers. The tuning performance could be improved by using a narrower spectrum light source—such as a laser or an OLED with reduced spectral width as demonstrated by Puzzo et al.[40] Another way to improve the tuning performance is to increase the shift of the stop band of the BS, i.e. by using materials with a higher TOC.[41] The highest TOCs in inorganic materials reach up to $\pm 10^{-4}$ K^{-1} and can be even higher in organic materials,[42,43] which mostly possess a negative TOC around -1 to -6×10^{-4} K^{-1} (it should be mentioned, however, that the thermal expansion in organic materials can have a counteracting effect on the shift of the stop band). Further improvements that need to be addressed are the device thermal capacity in order to increase device speed and thermal conductance in lateral directions. As we have seen in Figure 6, the heat conductivity across the device is fairly good which could be a problem for the image contrast. To prevent thermal crosstalk, the heat conduction in lateral dimensions can be suppressed by employing thinner substrates and a heat sink on the back side of the device. Though our active components only have a thickness of approximately 2.3 μm, the whole device measures currently 1.5 mm, which leaves room for improvement. The potentially low fabrication costs and optical readout leads to numerous possible applications. The imaging sensors can be provided by a mobile phone or a compact camera.

CONCLUSION

In this work we demonstrated an integrated detection platform based on an OLED and a photonic crystal, which is capable of infrared sensing via the temperature-induced spectral modulation of a thermoresponsive photonic crystal. On the basis of this sensing principle, the PC's thermal response translates into an intensity change in the transmitted light intensity, thus allowing for the straightforward realization of a greyscale detection scheme as opposed to the more conventional color readout schemes. Furthermore, we demonstrated time and spatially resolved temperature mapping on the device surface by interfacing the OLED-PC with a commercial CCD camera.

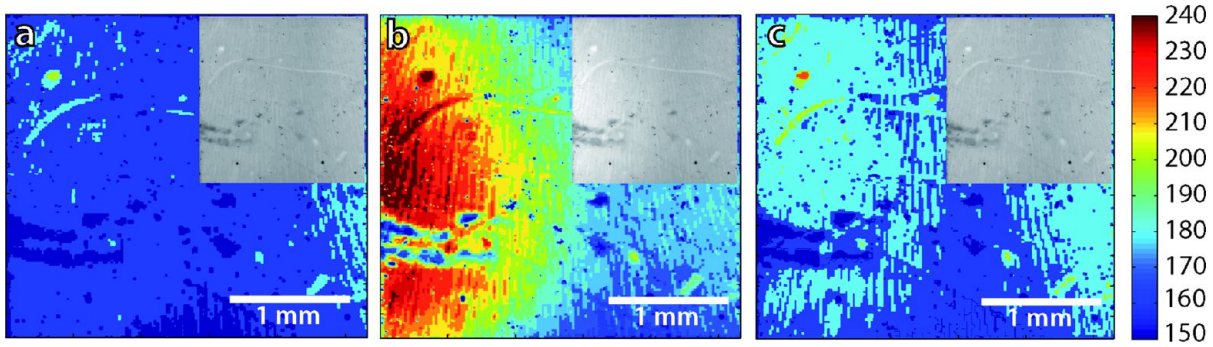

Figure 6. Colored optical images demonstrating the OLED shining through the BS in (a) thermal equilibrium at 27 °C and (b) heated on the left side. The insets show the corresponding raw image obtained by a monochrome CCD camera. (c) The OLED-BS, 10 s after heating at a temperature of 33 °C.

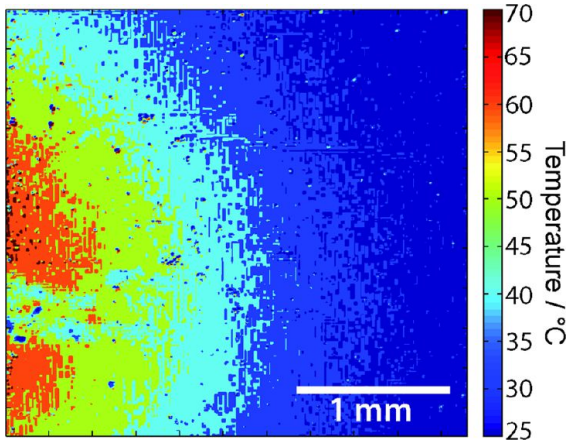

Figure 7. Calibrated thermogram, corresponding to Figure 6b, displaying the distribution of the OLED-BS temperature under the thermal gradient.

■ ASSOCIATED CONTENT

Supporting Information

Detailed fabrication and characterization methods. This material is available free of charge via the Internet at http://pubs.acs.org.

■ AUTHOR INFORMATION

Corresponding Author

*E-mail: lugli@tum.de.

Author Contributions

§These authors contributed equally to this work.

Notes

The authors declare no competing financial interest.

■ ACKNOWLEDGMENTS

This work was supported by the cluster of excellence "Nanosystems Initiative Munich" (NIM) as well as the Center for NanoScience (CeNS). The doctoral scholarships for Ida Pavlichenko granted by the Elite Network of Bavaria and for Armin Exner granted by the Institute of Advanced Study (IAS) and the International Graduate School of Science and Engineering (IGSSE) are gratefully acknowledged. We thank G. Derondeau, A. Folger, S. Menacher, and K. Szendrei for experimental assistance.

■ REFERENCES

(1) Rogalski, A. *Infrared Detectors*, Second ed.; CRC Press: Boca Raton, FL, 2010; p 898.
(2) Meola, C.; Carlomagno, G. M. *Meas. Sci. Technol.* **2004**, *15*, R27−R58.
(3) Rogalski, A. *Prog. Quant. Electron.* **2003**, *27*, 59−210.
(4) Rogalski, A. *Infrared Phys. Techn.* **2002**, *43*, 187−210.
(5) Rogalski, A. *Rep. Prog. Phys.* **2005**, *68*, 2267−2336.
(6) Dereniak, E. L.; Boreman, G. D. *Infrared detectors and systems*; Wiley: New York, 1996; p 561.
(7) Smith, E. P. G.; Winchester, K. J.; Musca, C. A.; Dell, J. M.; Faraone, L. *Semicond. Sci. Technol.* **2001**, *16*, 455−462.
(8) Walcott, T. M. *Bolometers: Theory, Types and Applications (Physics Research and Technology)*; Nova Science Publishers, Inc: Hauppage, NY, 2011.
(9) Ishikawa, T.; Ueno, M.; Nakaki, Y.; Endo, K.; Ohta, Y.; Nakanishi, J.; Kosasayama, Y.; Yagi, H.; Sone, T.; Kimata, M. Performance of 320 x 240 uncooled IRFPA with SOI diode detectors. In *Infrared Technology and Applications XXVI, Proceedings of SPIE*, San Diego, CA, July 30, 2000; Vol. *4130*, pp 152−159.
(10) El Mandouh, Z. *Thin Solid Films* **2000**, *371*, 259−263.
(11) Chen, C.; Yi, X.; Zhao, X.; Xiong, B. *Sens. Actuators* **2001**, *90*, 2000−2002.
(12) Wood, R. A.; Capper, P.; Elliott, C. T.; Willoughby, A. F. W.; Hull, R. *Infrared Detectors and Emitters: Materials and Devices*; Capper, P., Elliott, C. T., Eds.; Springer US: Boston, MA, 2001; Vol. *8*, pp 149−175.
(13) Sedky, S.; Fiorini, P.; Caymax, M.; Verbist, A.; Baert, C. *Sens. Actuators A-Phys.* **1998**, *66*, 193−199.
(14) Lavrik, N. V.; Grbovic, D.; Rajic, S.; Datskos, P. G.; Forrai, D.; Nelson, E.; Devitt, J.; McIntyre, B. Uncooled infrared imaging using bimaterial microcantilever arrays. In *Infrared Technology and Applications XXXII, Proceedings of SPIE*, Orlando, FL, April 17, 2006; Vol. *6206*, pp 62061K−62061K-8.
(15) Emmons, R. B.; Hawkins, S. R.; Cuff, K. F. *Opt. Eng.* **1975**, *14*, 21−30.
(16) Smith, R. A. *Detection and Measurement of Infrared Radiation (Monographs on the Physics & Chemistry of Materials)*; Oxford University Press: New York, 1968; p 522.
(17) Niklaus, F.; Kälvesten, E.; Stemme, G. *J. Micromech. Microeng.* **2001**, *11*, 509.
(18) Jones, C. D. W.; Bolle, C. A.; Ryf, R.; Simon, M. E.; Pardo, F.; Aksyuk, V. A.; Lai, W. Y.-C.; Bower, J. E.; Miner, J. F.; Klemens, F. P.; Cirelli, R. A.; Sorsch, T. W.; Ferry, E. J.; Fetter, L. A.; Pai, C.-S.; Taylor, J. A.; Vyas, B.; Watson, G. P.; Stekas, B.; Baker, M. R.; Papazian, A. R.; Basavanhally, N. R.; Mansfield, W. M.; Kornblit, A.; Keller, R. C.; Gates, J. V.; Ramirez, A. P. *Sens. Actuators A-Phys.* **2009**, *155*, 47−57.
(19) Ostrower, D. *III-Vs Rev.* **2006**, *19*, 24−27.
(20) Lavrik, N.; Archibald, R.; Grbovic, D.; Rajic, S.; Datskos, P. Uncooled MEMS IR imagers with optical readout and image

processing. In *Infrared Technology and Applications XXXIII, Proceedings of SPIE*, Orlando, FL, April 9, 2007; Vol. *6542*, p. 65421E−65421E-8.
(21) Grbovic, D.; Lavrik, N. V.; Datskos, P. G.; Forrai, D.; Nelson, E.; Devitt, J.; McIntyre, B. *Appl. Phys. Lett.* **2006**, *89*, 073118.
(22) Salerno, J. P. High frame rate imaging using uncooled optical readout photomechanical IR sensor. In *Infrared Technology and Applications XXXIII, Proceedings of SPIE*, Orlando, FL, April 9, 2007; Vol. *6542*, pp 65421D−65421D-9.
(23) LeMieux, M. C.; McConney, M. E.; Lin, Y.-H.; Singamaneni, S.; Jiang, H.; Bunning, T. J.; Tsukruk, V. V. *Nano Lett.* **2006**, *6*, 730−734.
(24) Watts, M. R.; Shaw, M. J.; Nielson, G. N. *Nature Photon.* **2007**, *1*, 632−634.
(25) Joannopoulos, J. D. *Photonic Crystals: Molding The Flow Of Light*; 2nd ed.; Princeton University Press: Princeton, NJ, 2008; p 286.
(26) Calvo, M. E.; Colodrero, S.; Hidalgo, N.; Lozano, G.; López-López, C.; Sánchez-Sobrado, O.; Míguez, H. *Energy. Environ. Sci.* **2011**, *4*, 4800.
(27) Pris, A. D.; Utturkar, Y.; Surman, C.; Morris, W. G.; Vert, A.; Zalyubovskiy, S.; Deng, T.; Ghiradella, H. T.; Potyrailo, R. A. *Nature Photon.* **2012**, *6*, 195−200.
(28) Sambles, J. R. *Nature Photon.* **2012**, *6*, 141−142.
(29) Macleod, H. A. *Thin-film optical filters*; Hilger: Bristol, U.K., 1986; pp 1−519.
(30) Pavlichenko, I.; Exner, A. T.; Guehl, M.; Lugli, P.; Scarpa, G.; Lotsch, B. V. *J. Phys. Chem. C.* **2012**, *116*, 298−305.
(31) Regoliosi, P.; Guehl, M.; Scarpa, G.; Lugli, P.; Persano, L.; Carro, P. D.; Camposeo, A.; Cingolani, R.; Pisignano, D.; Bietti, S.; Grilli, E.; Guzzi, M. *Appl. Phys. Lett.* **2008**, *92*, 2008−2010.
(32) Kim, D. Y.; Choudhury, K. R.; Lee, J. W.; Song, D. W.; Sarasqueta, G.; So, F. *Nano Lett.* **2011**, *11*, 2109−13.
(33) Takeoka, Y.; Watanabe, M. *Adv. Mater.* **2003**, *15*, 199−201.
(34) Weissman, J. M.; Sunkara, H. B.; Tse, A. S.; Asher, S. A. *Science (80-)* **1996**, *274*, 959−963.
(35) Colodrero, S.; Ocaña, M.; Míguez, H. *Langmuir* **2008**, *24*, 4430−4.
(36) Gülşen, G.; Naci Inci, M. *Opt. Mater.* **2002**, *18*, 373−381.
(37) Lee, Y.-F.; Chang, K.-H.; Chu, C.-Y.; Chen, H.-L.; Hu, C.-C. *RSC Adv.* **2011**, *1*, 401.
(38) Pavlichenko, I.; Exner, A. T.; Logvenov, G.; Scarpa, G.; Lugli, P.; Lotsch, B. V. *Can. J. Chem.* **2012**, *90* (12), 1069−1077.
(39) Minkina, W.; Dudzik, S. *Infrared Thermography: Errors and Uncertainties*; John Wiley and Sons: New York, 2009; p 212.
(40) Puzzo, D. P.; Helander, M. G.; O'Brien, P. G.; Wang, Z.; Soheilnia, N.; Kherani, N.; Lu, Z.; Ozin, G. A. *Nano Lett.* **2011**, *11*, 1457−1462.
(41) Kang, E.-S.; Lee, T.-H.; Bae, B.-S. *Appl. Phys. Lett.* **2002**, *81*, 1438.
(42) Ballato, J.; James, A. *J. Am. Ceram. Soc.* **1999**, *82*, 2273−2275.
(43) Zhang, Z.; Zhao, P.; Lin, P.; Sun, F. *Polymer* **2006**, *47*, 4893−4896.